SIAM J. APPL. MATH.
Vol. 63, No. 2, pp. 722–744

THIN FILM TRAVELING WAVES AND THE NAVIER SLIP CONDITION*

ROBERT BUCKINGHAM†, MICHAEL SHEARER‡, AND ANDREA BERTOZZI§

Abstract. We consider the lubrication model for a thin film driven by competing gravitational forces and thermal gradients on an inclined plane. We are interested in the general traveling wave problem when the Navier slip boundary condition is used. We contrast (1) gravity dominated flow, (2) Marangoni dominated flow, and (3) flow in which the two driving effects balance. For a "singular slip" model we show that when Marangoni forces are present the resulting traveling wave ODE reduces locally near the contact line to a case not considered previously in the literature. We compute an asymptotic expansion of the solution near the contact line and compare with numerical simulations of the full problem. Using numerical simulations and phase space analysis involving Poincaré sections, we show that for all three problems there is a finite range of admissible contact angles for which traveling wave solutions exist. Even in the well-studied case (1), this is a new observation that has ramifications for the use of constitutive laws at the contact line in the case of singular slip. For case (3) multiple traveling wave solutions are observed with the same contact angle.

Key words. thin liquid films, contact lines, traveling waves, nonlinear partial differential equations

AMS subject classifications. 35K55, 35Q35, 76D08, 76D45, 34C37

PII. S0036139902401409

Introduction. Dynamic contact lines occur at the leading edge of a layer of fluid coating a dry solid surface. Understanding how contact lines move has been the subject of intense interest for several decades. In particular, it was shown by Dussan and Davis [13] that motion necessarily implies a singularity of stress at the contact line if the usual no-slip boundary condition is imposed between the fluid and the solid surface. Two approaches to removing this singularity emerged early on, namely (i) the precursor layer model and (ii) the Navier slip condition.

In 1964, Bascom, Cottington, and Singleterry [1] reported experimental observations of contact lines for thin liquid films. A very thin film was observed spreading ahead of the thicker film, beyond the apparent location of the contact line. Based on these and similar observations, one reasonable model is to assume that there is a very thin layer of fluid ahead of the contact line. The contact line itself is then replaced by a rapid transition from the thicker layer to the very thin layer. This is the basis for the so-called *precursor model* studied in various contexts over a number of years. While this is an attractive and tractable way to remove the singularity associated with the film thickness going all the way to zero, modeling the very thin precursor layer using hydrodynamics can be questionable since its thickness is only a

*Received by the editors January 23, 2002; accepted for publication (in revised form) June 24, 2002; published electronically January 14, 2003.
http://www.siam.org/journals/siap/63-2/40140.html
†Department of Mathematics, Duke University, Durham, NC 27708 (robbie@math.duke.edu). The research of this author was supported by NSF grants DMS-9983320 and DMS-0074049.
‡Center for Research in Scientific Computation and Department of Mathematics, North Carolina State University, Raleigh, NC 27695-8205 (shearer@math.ncsu.edu). The research of this author was supported by National Science Foundation grant DMS-0073841 and by Army Research Office grant DAAG55-98-10128.
§Departments of Mathematics and Physics, Duke University, Durham, NC 27708 (bertozzi@math.duke.edu). The research of this author was supported by NSF grant DMS-0074049 and ONR grant N000140110290.

few Ångstroms. Within a continuum framework, this can be approached by including additional physics, such as long range van der Waals forces [12, 34, 41] in a dynamic model of the precursor layer itself (as in [16]).

The second approach that has received extensive study is to keep the distinct contact line but remove the stress singularity by modifying the boundary condition between the liquid and the solid surface at or near the contact line. The most promising way to do this is to introduce the *Navier slip condition*, proposed by Navier [32] in 1832 during the long debate over whether a fluid can slide over a solid surface [15]. The Navier condition was apparently first invoked in the context of lubrication theory by Greenspan [17] and has since been included in numerous studies of contact lines [2, 22, 31, 38, 39]. Again, this is an attempt to resolve the issue using only hydrodynamics, rather than dealing with the atomic scale forces that are undoubtedly significant near the contact line. Nonetheless, it is plausible to believe that the effect of these forces at the macroscopic scale could be captured in an empirical law like the Navier slip condition. Once a choice of slip model is made, there is still the question of the need for a boundary condition at the contact line. Greenspan [17] proposed that the speed of the contact line is related to the contact angle. This was further considered for spreading drops by Haley and Miksis [18] and Ehrhard and Davis [14]. Hocking [23] considers using the static contact angle for the dynamic problem. In the case of complete wetting, a zero contact angle solution is preferred. For the general lubrication PDE, existence of such "zero contact angle" solutions with slip was proved rigorously in one space dimension [3, 8]. In this case, the zero contact angle condition replaces the boundary condition or fixed contact angle condition at the contact line. A natural question, which we address, is whether the PDE admits traveling wave solutions with a prescribed nonzero contact angle condition.

In this paper, we consider a thin film being driven up an inclined solid surface by a surface or Marangoni stress. These driven films have been studied extensively theoretically, experimentally, and numerically [5, 6, 10, 11, 27, 28, 29, 37, 36]. In particular, in a series of papers on the precursor model, we found interesting novel structures for traveling waves and their stability [4, 6, 7]. Our purpose in this paper is to explore the Navier slip model as an alternative to the precursor model for Marangoni driven films. Among other conclusions, we find that for a given slip length and film thickness, there is a finite range of contact angles that admit traveling wave solutions.

In section 2, we give a brief derivation of the fourth order nonlinear PDE governing the evolution of film height, using the lubrication approximation to the Navier–Stokes equations for two-dimensional incompressible flow. This derivation shows how the Navier slip condition enters the thin film PDE. Also in section 2 we show how traveling wave solutions with a contact line satisfy a third order ODE, in which the traveling wave speed is determined by the upstream height. The PDE and associated traveling wave ODE can be used to study contact lines under three scenarios, each of which we consider in this paper:

I. Flow in which gravity is the only driving force. For example, a layer of fluid wetting a dry surface as it slides down the surface under the action of gravity.

II. Flow in which the Marangoni force dominates gravity.

III. Flow in which Marangoni force and the force due to gravity are balanced.

The main results of this paper, both analytical (in section 3) and numerical (in section 4) concern flow in which forces are balanced, but our numerical results add something to the understanding of the first two scenarios as well.

In section 3 we analyze the traveling wave ODE near the contact line when Marangoni forces are present, under the Navier slip condition. Curiously, the leading order terms of the ODE are independent of the precise form of the Navier slip condition; we are led to the problem of finding a function $y = y(x)$ (representing the film height) that is positive for $x > 0$ and satisfies

$$yy''' = 1, \quad x > 0, \quad y(0) = 0. \tag{1.1}$$

This equation would appear to fall under the extensive classification of solutions of the more general third order ODE $y^n y''' = 1$ contained in the paper of Boatto, Kadanoff, and Olla [9]. However, we observe that the case $n = 1$ is special, and we find a different structure for the solutions. In section 3.1, we find a two-parameter family of asymptotic solutions

$$y(x) = ax + \frac{1}{2a}x^2 \log x + bx^2 + \text{h.o.t.}, \tag{1.2}$$

where h.o.t. denotes higher order terms and $a > 0$ and b are free parameters. We show how the series can be continued indefinitely, and in section 3.1 we perform a reduction to a polynomial planar vector field that establishes the dimension of the solution set.

In section 4 we present various results of numerical integration of the third order traveling wave ODE. The technique we use is similar to that in earlier studies of the precursor layer model [6], but here we show how the entire phase space can be understood by focusing on the structure of stable and unstable invariant manifolds associated with equilibria. Phase portraits are three-dimensional, since the ODE is third order, so we visualize invariant manifolds through their intersection with carefully chosen Poincaré sections.

The numerical solutions are compared with the asymptotic form (1.2) near the contact line. The numerical results highlight various interesting issues. We find a finite range of contact angles for each wave speed. This has relevance for the use of a boundary condition relating contact angle and wave speed, as considered in [14, 18], or for the case of a fixed contact angle condition, as considered in [31, 38] for singular slip and in [20, 21, 23] for nonsingular slip. Moreover, at a given speed and at a given contact angle in this range, there may be several different traveling waves. The latter property is specific to the case in which gravity and Marangoni effects balance and is related to the nonconvexity of the flux function in the lubrication model. This particular effect is well understood for the same problem in which a simpler precursor film model is used to remove the contact line singularity [6].

2. The lubrication approximation and traveling waves. In section 2.1, we outline the lubrication approximation and formulate the PDE that governs the motion of the thin liquid layer, including the Navier slip condition. In section 2.2, we derive a third order ODE whose solutions are traveling wave solutions of the PDE.

2.1. The thin film PDE. Consider a thin liquid film moving slowly up a flat solid surface, inclined at an angle α to the horizontal. The film is driven by a constant surface stress τ, and gravity also acts on the film, as indicated in Figure 2.1. We shall consider the film to be uniform in the transverse direction. This means that the transverse velocity is zero, the in-plane velocity (u, v) and pressure p are functions of x, z, and time t, and the free surface is given by $z = h(x, t)$, where h is a function to be determined. The lubrication approximation reduces the description of the flow to a PDE for $h(x, t)$.

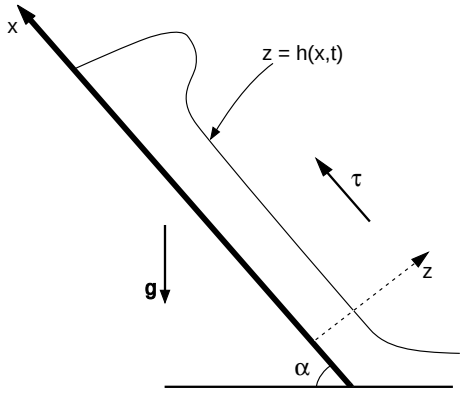

FIG. 2.1. *Thin film propagating up an inclined solid surface.*

The Navier–Stokes equations for the two-dimensional flow of the figure are as follows:

$$\begin{aligned} &\text{(a)} && \rho(u_t + uu_x + vu_z) = -p_x + \mu(u_{xx} + u_{zz}) - \rho g \sin\alpha, \\ &\text{(b)} && \rho(v_t + uv_x + vv_z) = -p_z + \mu(v_{xx} + v_{zz}) - \rho g \cos\alpha, \\ &\text{(c)} && u_x + v_z = 0. \end{aligned} \tag{2.1}$$

Here, ρ is the density, taken to be constant, consistent with the incompressibility condition (2.1c), and μ is the viscosity.

In the lubrication approximation, we exploit two small quantities to reduce the complexity of the equations, keeping only leading order terms but maintaining a balance between terms that are significant, namely surface stresses and viscous forces. Let H be a typical thickness of the film, say a maximum thickness. This is assumed small compared to a typical length scale L along the solid surface. The other small parameter is the Reynolds number $Re = \rho UH/\mu$, calculated with respect to the thickness length scale, but where U is a typical velocity in the x-direction parallel to the solid surface.

The lubrication approximation that emerges as the leading order terms consists of two equations, with unknowns velocity u parallel to the solid surface and pressure p (the normal velocity v is given separately by the incompressibility condition (2.1c)):

$$\begin{aligned} &\text{(a)} && p_x = \mu u_{zz} - \rho g \sin\alpha, \\ &\text{(b)} && p_z = -\rho g \cos\alpha. \end{aligned} \tag{2.2}$$

To this system we add boundary conditions at $z = 0$ and $z = h$:

$$\begin{aligned} &\text{(a)} && p = p_A - \gamma h_{xx} && \text{on} \quad z = h, \\ &\text{(b)} && \mu u_z = \tau && \text{on} \quad z = h, \\ &\text{(c)} && k(h)u_z = u && \text{on} \quad z = 0. \end{aligned} \tag{2.3}$$

Here, p_A denotes atmospheric pressure, γ is the coefficient of surface tension, taken

to be constant, τ is a constant surface stress[1] coupled to the flow by the rate of shear strain appearing on the left-hand side of (2.3b). (Other mechanisms produce a surface stress, such as gradients in the concentration of a surfactant or airflow over the surface.) The boundary condition (2.3c) expresses the Navier slip condition, in which $k(h)$ is a coefficient with dimension of length that becomes essentially zero away from the contact line (i.e., for $h > h_0$ where h_0 is small). As in earlier work on the Navier slip condition, we take $k(h)$ to be a smooth and positive function; it would be possible to cut $k(h)$ off at a specified distance from an advancing contact line. For simplicity we choose only smooth functions $k(h)$ as in [17, 18, 39, 31]. Specific forms for $k(h)$ will be given later.

To derive an equation for $h(x,t)$, we first integrate system (2.2) using the boundary conditions (2.3) to obtain an expression for u in terms of z and h. Then u is averaged across the film to get an average velocity Q, expressed entirely in terms of h and derivatives of h. Finally, this formula for Q is substituted into the equation

$$h_t + (hQ)_x = 0$$

expressing conservation of mass. This procedure, explained in detail and in greater generality elsewhere [17, 31], leads to the single equation

$$h_t + \left\{ \frac{\tau}{2\mu} q(h) - \frac{\rho g \sin\alpha}{3\mu} c(h) - \frac{\rho g \cos\alpha}{3\mu} c(h) h_x + \frac{\gamma}{3\mu} c(h) h_{xxx} \right\}_x = 0, \tag{2.4}$$

in which

$$q(h) = h^2 + 2hk(h), \quad c(h) = h^3 + 2h^2 k(h) \tag{2.5}$$

would be quadratic and cubic functions (respectively) were it not for the modifications from the Navier slip condition.

From (2.4) we can realize the three cases of the introduction:

1. Gravity dominates: $\tau = 0$.
2. Marangoni forces dominate: $\tau >> \rho g \sin\alpha$.
3. Gravity and Marangoni effects are in balance: $\tau \sim \rho g \sin\alpha$.

In each case, a slightly different scaling of the variables leads to nondimensional equations. We give the details in the third case, rescaling the variables as in [6]. We introduce length scales H, L and a corresponding time scale T:

$$h = H\hat{h}, \quad x = \hat{x}L, \quad \text{and} \quad t = T\hat{t}. \tag{2.6}$$

Balancing the competing convective effects of gravity and Marangoni forces in (2.4) gives $H = \frac{3\tau}{2\sin\alpha\rho g}$. Setting L to be the capillary length on which surface tension balances the driving forces gives $L = (\frac{2\gamma H^2}{3\tau})^{1/3} = (\frac{3\gamma\tau}{2\rho^2 g^2 \sin^2\ a})^{1/3}$. The time scale is then chosen to be the one on which all three of these effects balance, $T = 2\frac{\mu}{\tau^2}(\frac{4}{9}\tau\gamma\rho g\sin\alpha)^{1/3}$.

This leads to the equation

$$\begin{aligned} h_t + \left(\left(h^2 + \frac{2}{3} h K(h) \right) - (h^3 + h^2 K(h)) \right)_x \\ = D\left((h^3 + h^2 K(h)) h_x \right)_x - \left((h^3 + h^2 K(h)) h_{xxx} \right)_x, \end{aligned} \tag{2.7}$$

[1]Here, we assume a constant surface tension gradient, proportional to the constant temperature gradient in experiments [37, 36], in the regime in which surface tension depends linearly upon temperature.

where $D = \frac{\rho g \cos\alpha\, T H^3}{3\mu L}$ and

$$K(h) = \frac{3k(Hh)}{H}. \tag{2.8}$$

We remark that D is typically small and is zero for a vertical plane ($\alpha = \pi/2$). It will be convenient to label the flux $f(h)$ on the left-hand side of (2.7),

$$f(h) = \left(h^2 + \frac{2}{3}hK(h)\right) - (h^3 + h^2K(h)), \tag{2.9}$$

and to use the notation

$$C(h) = h^3 + h^2K(h). \tag{2.10}$$

Then the depth-averaged velocity Q is given by

$$Q = (f(h) - DC(h)h_x + C(h)h_{xxx})/h, \tag{2.11}$$

and the PDE (2.7) is

$$h_t + f(h)_x = D(C(h)h_x)_x - (C(h)h_{xxx})_x. \tag{2.12}$$

In cases 1 and 2, a similar rescaling leads to equations similar to (2.12) but with different flux functions $f(h)$ (see [31]). Specifically:

1. When gravity dominates, the thin film will be coating by flowing down the solid surface. Reversing x so that increasing x is in the direction of flow, we obtain (2.12) with

$$f(h) = h^3 + h^2K(h). \tag{2.13}$$

2. When Marangoni forces dominate, the gravity term in the flux drops out, and we are left with

$$f(h) = h^2 + hK(h). \tag{2.14}$$

2.2. Traveling waves. We seek traveling wave solutions of (2.12). These take the form $h(x,t) = \overline{h}(x - st)$, where $\overline{h}$ is a function of the single traveling wave variable $\xi = x - st$, and s is the wave speed. Substituting into the PDE, and integrating once, we obtain (dropping the bars)

$$E - sh + f(h) = DC(h)h' - C(h)h''', \tag{2.15}$$

in which $'$ denotes differentiation with respect to ξ, and E is the constant of integration.

Now we are interested particularly in solutions that have a contact line, at which $h = 0$. Since the ODE is autonomous, we can assume the contact line is at $\xi = 0$. Upstream (i.e., $\xi \longrightarrow -\infty$), we assume the traveling wave approaches a constant height, with at least the first three derivatives approaching zero. Thus, we have boundary conditions

$$h(-\infty) = h_-, \qquad h'(-\infty) = h''(-\infty) = h'''(-\infty) = 0, \qquad h(0) = 0. \tag{2.16}$$

Letting $\xi \longrightarrow -\infty$, we find $E = sh_- - f(h_-)$.

At the other end, letting $\xi \longrightarrow 0-$, we have $Q \longrightarrow s$. (I.e., the average speed approaches the speed of the traveling wave at the contact line.) Using (2.11), we can rewrite (2.15) as

$$-s + Q(h) = E/h.$$

Letting $h \longrightarrow 0$ leads to the conclusion $E = sh_- - f(h_-) = 0$. Thus, the wave speed *s is determined by the upstream height h_-*:

$$s = \frac{f(h_-)}{h_-}. \tag{2.17}$$

In conclusion, the traveling wave satisfies the ODE

$$C(h)h''' = sh - f(h) + DC(h)h', \tag{2.18}$$

with boundary conditions

$$h(-\infty) = h_-, \quad h(0) = 0. \tag{2.19}$$

Finally, we discuss the leading order terms at the contact line in (2.18). To do so, we need to specify the constitutive function $k(h)$ in the Navier slip condition (2.3c). The form of this function is not decided upon [17, 18], but the idea is that slip should be confined to a small neighborhood of the contact line, where h is very small. Thus, $k(h)$ should be chosen so that it is nearly zero unless h is very small. Typically, $k(h)$ is chosen to be a power of h; in order to satisfy the above requirement, this power should be negative. Thus we take

$$k(h) = \eta h^{n-2}, \tag{2.20}$$

with $n < 2$ and $\eta > 0$. In [17], the choice is $n = 1$. This slip model was derived by Neogi and Miller for flow over a porous surface [33]. Other choices are possible, including $n = 2$ which can model polymer flow [12]. Note that for $n > 2$, $k(h)$ grows away from the contact line. With the choice (2.20), the function $K(h)$ defined in (2.8) becomes

$$K(h) = \beta h^{n-2}, \tag{2.21}$$

with $\beta = 3\eta H^{n-3}$. In particular, there are two parameters in this relation, namely β and n.

Now consider the leading order terms as $h \longrightarrow 0$, i.e., near the contact line. We have $C(h) = h^3 + h^2K(h) \sim \beta h^n$. Asymptotics for $f(h)$ depend on which case we are considering. In case 1, in which gravity dominates, $f(h) = h^3 + h^2K(h) \sim \beta h^n$. In case 2 and case 3, the terms from the Marangoni force are higher order. Specifically in case 3, $f(h) = (h^2 + \frac{2}{3}hK(h)) - (h^3 + h^2K(h)) \sim \frac{2}{3}\beta h^{n-1}$.

Retaining leading order terms in the ODE, we get, in case 1, the equation

$$\beta h^{n-1}h''' = s + \beta h^{n-1} + D\beta h^{n-1}h'. \tag{2.22}$$

Thus, for case 1, the choice $n = 1$ leads to a constant coefficient equation. Notably, there is then no singularity at $h = 0$.

In cases 2 and 3, we obtain the singular equation

$$hh''' = -\frac{2}{3} + Dhh'. \tag{2.23}$$

At the contact line, we expect h' to be finite (although it would be reasonable to consider solutions with a vertical tangent at the contact line). Moreover, the parameter D will be considered small or zero. Thus, we take $Dhh' \sim 0$ to leading order. Note that in arriving at (2.23), we have depended on two important assumptions: (1) There is a surface driving force $\tau > 0$, and (2) $n < 2$ in (2.20).

Rescaling ξ in (2.23), and dropping the last term, we are led to consider the initial value problem

$$yy''' = 1, \quad y(x) > 0 \quad \text{for} \quad x > 0, \quad y(0) = 0, \tag{2.24}$$

in which $x = -(\frac{2}{3})^{1/3}\xi$ and $y(x) = h(\xi)$.

3. Solutions near the contact line. In this section we explore properties of the initial value problem (2.24). In subsection 3.1 we establish an asymptotic series solution that has two free parameters, and in subsection 3.2 we reduce the third order equation to a planar vector field, whose phase portrait proves the existence of a two-parameter family of solutions.

3.1. Asymptotics. In this subsection, we elaborate on the proposed family (1.2) of solutions of (2.24) and show how the terms of an asymptotic series can be calculated systematically. To this end, consider the series[2]

$$y(x) = ax + \frac{1}{2a}x^2 \log x + bx^2 + \Sigma(x), \tag{3.1}$$

where $\Sigma(x)$ is expressed as a series with coefficients to be determined:

$$\Sigma(x) = \sum_{k=3}^{\infty} \sum_{j=2}^{k} d_{k\,j} x^k (\log\, x)^{k-j}. \tag{3.2}$$

Note that the series is organized as a sum of terms of increasing order (as $x \to 0+$). We will show that the coefficients $d_{k\,j}$ may be calculated in the same order: $d_{32}, d_{33}, d_{42}, d_{43}, d_{44}, d_{52}, \ldots$. In what follows, it will be helpful to adopt the convention that $d_{km} = 0$ whenever $m \le 1$.

Consider a single term $z_{kj}(x) = x^k (\log\, x)^{k-j}$ with $k \ge 3, 2 \le j \le k$. Then

$$z_{kj}''' = x^{k-3} \left\{ A_k (\log\, x)^{k-j} + B_{kj} (\log\, x)^{k-j-1} + C_{kj} (\log\, x)^{k-j-2} + A_{k-j} (\log\, x)^{k-j-3} \right\},$$

where the coefficients A, B, C are nonnegative; most importantly $A_k > 0$ for $k \ge 3$. They are given by the formulae

$$A_k = \begin{cases} k(k-1)(k-2) & \text{if} \quad k \ge 3, \\ 0 & \text{if} \quad k \le 2, \end{cases} \qquad B_{kj} = \begin{cases} (3k^2 - 6k + 2)(k-j) & \text{if} \quad k > j, \\ 0 & \text{if} \quad k \le j, \end{cases}$$

$$C_{kj} = \begin{cases} 3(k-1)(k-j)(k-j-1) & \text{if} \quad k \ge j+2, \\ 0 & \text{if} \quad k \le j+1. \end{cases}$$

[2]Hocking [19] considered a leading order expansion of this form for a correction to the trailing edge of Huppert's solution [24] for flow down an inclined plane.

Thus

$$\begin{aligned} y''' &= \frac{1}{ax} + \sum_{k=3}^{\infty}\sum_{j=2}^{k} d_{kj} z'''_{kj} \\ &= \frac{1}{ax} + x^{-3}\sum_{k=3}^{\infty}\sum_{j=2}^{k} \alpha_{kj} x^k (\log\, x)^{k-j}, \end{aligned} \tag{3.3}$$

where the coefficients α_{kj} are linear combinations of the d_{kj}'s:

$$\alpha_{kj} = A_k d_{kj} + B_{kj-1} d_{kj-1} + C_{kj-2} d_{kj-2} + A_{k-(j-3)} d_{kj-3}. \tag{3.4}$$

(Recall $d_{km} = 0$ if $m \le 1$.)

Now substitute (3.1), (3.3) into (1.1):

$$\begin{aligned} &\left[ax + \frac{1}{2a}x^2 \log x + bx^2 + \sum_{k=3}^{\infty}\sum_{j=2}^{k} d_{kj} x^k (\log\, x)^{k-j}\right] \\ &\qquad \times \left[\frac{1}{ax} + \sum_{k=3}^{\infty}\sum_{j=2}^{k} \alpha_{kj} x^{k-3} (\log\, x)^{k-j}\right] = 1. \end{aligned} \tag{3.5}$$

Equating terms, we get a family of equations for the coefficients d_{kj} (recall the coefficients α_{kj} depend linearly on the d's):

$$\begin{aligned} x\log x: &\qquad \frac{1}{2a^2} + a\alpha_{32} = 0, \\ x: &\qquad \frac{b}{a} + a\alpha_{33} = 0, \end{aligned} \tag{3.6}$$

$x^{k-2}(\log x)^{k-j}$:

$$a\alpha_{kj} + \tfrac{1}{2a}\alpha_{k-1j} + b\alpha_{k-1j-1} + \tfrac{1}{a} d_{k-1j-1} + \sum_{m+p=k+1}\ \sum_{n+q=j+1} d_{mn}\alpha_{pq} = 0. \tag{3.7}$$

In the final sum, the additional constraints on the indices are implied from (3.5):

$$m \ge 3, \quad p \ge 3, \quad 2 \le n \le m, \quad 2 \le q \le p.$$

In particular, these imply

$$m \le k-2 \quad \text{and} \quad p \le k-2. \tag{3.8}$$

Also note that there is no contribution from the double sum if $k = 4$, or when $j = 2$.

Now from (3.4), we observe that the equation for the coefficient of $x^{k-2}(\log x)^{k-j}$ has a term $aA_k d_{kj}$, and the other terms involve d_{km} with $m \le j-1$ (these terms come from α_{kj}) and d_{mq} with $m \le k-1, 2 \le q \le m$. Consequently, the equations can be solved successively for the coefficients d_{kj} in their natural order associated with terms of increasing order in the asymptotic expansion. Thus, the asymptotic series can be continued to all orders and defines a two-parameter family of formal solutions of the ODE (1.1).

3.2. Reduction to a planar vector field. In this subsection, we reduce the ODE to a planar vector field that we analyze directly. While this is not a new technique (see, for example, [9, 40], where similar reductions are performed on other third order ODEs related to similarity solutions of thin film equations), the real interest lies in using the planar vector field to identify a family of solutions of the ODE with the two-parameter family of asymptotic solutions in the previous subsection.

Consider the ODE (1.1):

$$yy''' = 1. \tag{3.9}$$

Since this equation is autonomous and has a natural scaling invariance (scaling x by a^2 and y by a^3 leaves the equation unchanged), we can reduce the equation to a second order equation that is also autonomous. This is achieved by writing $w = y'$ and letting the independent variable be y. Thus, (3.9) becomes the second order equation

$$yw\frac{d}{dy}w\frac{dw}{dy} = 1. \tag{3.10}$$

Now $y\frac{d}{dy}$ is the logarithmic derivative, so we redefine the independent variable as $\eta = \log y$, leading to

$$w\frac{d}{d\eta}w\frac{dw}{d\eta} = w^2\frac{dw}{d\eta} + e^\eta. \tag{3.11}$$

Now we write this equation as a first order system and rescale to make it autonomous. First let $v = w\frac{dw}{d\eta}$. Then

$$w\frac{dv}{d\eta} = e^\eta + vw, \quad w\frac{dw}{d\eta} = v. \tag{3.12}$$

Now we remove the singularity at $w = 0$ (or rather send it to infinity) by letting $u = 1/w$. Then

$$\frac{du}{d\eta} = -u^3v, \quad \frac{dv}{d\eta} = e^\eta u + v. \tag{3.13}$$

Finally we scale the variables to make the system autonomous:

$$U = e^{\eta/3}u, \qquad V = e^{-2\eta/3}v,$$

leading to the system

$$U' = \frac{1}{3}U - U^3V, \quad V' = U + \frac{1}{3}V. \tag{3.14}$$

In terms of the original variables, x, y, we have $U = y^{1/3}/y'$, $V = y^{1/3}y''$. The asymptotic form (1.2) of the solutions approaching $y = 0$ yields

$$U \sim a^{-2/3}x^{1/3} \longrightarrow 0+, \qquad V \sim a^{-2/3}x^{1/3}\log x \longrightarrow 0- \tag{3.15}$$

as $x \longrightarrow 0+$. Note that $V/U \sim \log x \longrightarrow -\infty$ as $x \longrightarrow 0+$. Thus we are interested in solutions of (3.14) approaching the origin as the independent variable $\eta = \log y$ approaches $-\infty$, with $U(\eta) > 0, V(\eta) < 0$.

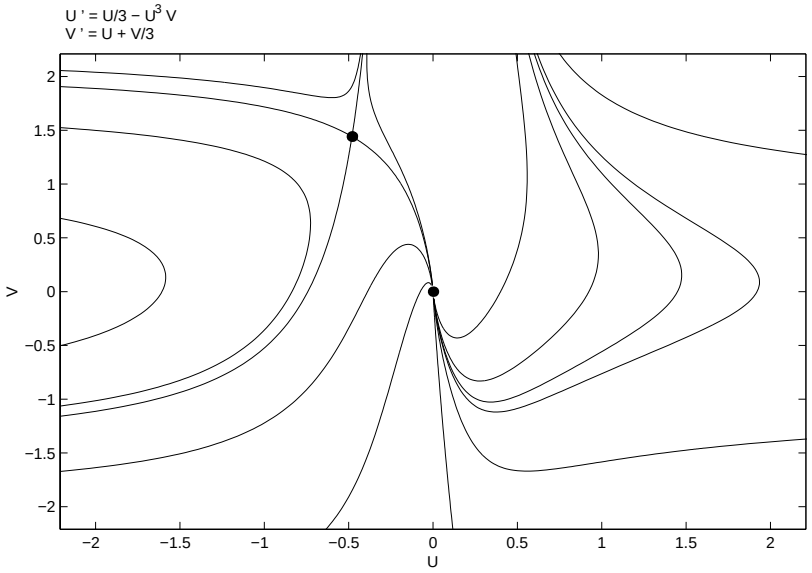

FIG. 3.1. *Phase portrait for system* (3.14).

The origin is an equilibrium with a double eigenvalue $1/3$, but a single eigenvector $(U, V) = (0, 1)$. The phase portrait is shown in Figure 3.1. Note that the saddle point at $V = -3U, U = -3^{-2/3}$ in the second quadrant is not relevant to us. The stable and unstable manifolds correspond to solutions with $y \longrightarrow \infty$ or $y \longrightarrow 0-$. It is straightforward to prove that the trajectories in the fourth quadrant have a unique minimum as they cross $V = -3U$ and cross the U axis as shown in the figure. Indeed, $dV/dU = 3$ on the U axis and is zero on the line $V = -3U$. Moreover,

$$\frac{dV}{dU} = \frac{U + \frac{1}{3}V}{\frac{1}{3}U - U^3V} < 3$$

and is positive for $U > 0,\ V < 0$. Thus, trajectories terminating at any point $U_1 > 0$ on the U axis are monotonically increasing from a point $(U_0, -3U_0)$ with $0 < U_0 < U_1$ and decrease monotonically to the left of the line $V = -3U$. However, the V axis is invariant for the vector field (3.14), so the trajectories are forced into the origin as η decreases. On every ray $V = -AU$ with $A > 3$, we have

$$\frac{dV}{dU} = \frac{U + \frac{1}{3}V}{\frac{1}{3}U - U^3V} > -A.$$

Consequently, trajectories cross every such ray as they approach the origin, proving that $dV/dU \longrightarrow -\infty$ as $\eta \longrightarrow -\infty$. In fact, neglecting the U^3V term as trajectories approach the origin, we find $V \sim 3U \log(U/U_0)$ as $U \longrightarrow 0+$.

This analysis of the fourth quadrant of the vector field proves that there is a one-parameter family of trajectories parameterized by $U_0 > 0$. The trajectories are also invariant under translation of η by a constant, since system (3.14) is autonomous. But $\eta = \log y$, so this corresponds to multiplying y by a constant, accompanied by the corresponding scaling of x, according to the natural scale invariance of (1.1). This is the second parameter that is apparent in the asymptotic series. We have thus proved the following proposition.

PROPOSITION 3.1. *There is a two-parameter family of solutions of the initial value problem* (1.1).

4. Numerical results. In this section, we show results of numerical simulations of the full traveling wave ODE in the spirit of [6]. In particular, we illustrate how solutions corresponding to contact lines relate to the parameters a, b in the asymptotic expansion derived in section 3.1, but we also explore the two simpler cases 1 and 2, in which gravity or the Marangoni forces dominate, respectively.

It is convenient to write the third order equation as a first order system, in which we replace h by u:

$$\begin{aligned} u' &= v, \\ v' &= w, \\ w' &= g(u, v, s), \end{aligned} \tag{4.1}$$

where $g(u, v, s) = \frac{su - f(u)}{C(u)} + Dv$.

The main parameter s is the traveling wave speed. We take $D = 0$, corresponding to fluid flowing down a vertical wall. The functions f, C were given in section 2:
Case I (gravity dominates): $f(u) = u^3 + u^2 K(u)$.
Case II (Marangoni force dominates): $f(u) = u^2 + uK(u)$.
Case III (gravity and Marangoni force are comparable): $f(u) = u^2 - u^3 + K(u)(\frac{2}{3}u - u^2)$.
Recall also the formulae for C and K:

$$C(u) = u^3 + K(u)u^2, \quad K(u) = \beta u^{n-2}. \tag{4.2}$$

In the function K, there are additional parameters $\beta > 0$ and $n < 2$; generally, we take $n = 1$ and $\beta = 0.01$, but we shall also consider the effect of varying β.

Equilibria of system (4.1) are $(u, v, w) = (\overline{u}, 0, 0)$, with $g(\overline{u}, 0, s) = 0$. I.e.,

$$f(\overline{u}) = s\overline{u}. \tag{4.3}$$

We study all the stable and unstable manifolds of equilibria, their boundaries, intersections, and behavior at $u = 0$ in order to gain some understanding of the overall phase portrait.

Computational algorithm. Trajectories for (4.1) are computed using the implicit Adams method in the LSODE package. To compute trajectories along a stable manifold starting near an equilibrium, we integrate backward in time. As for computing trajectories forward in time along an unstable manifold, this process is stable until the manifold comes near another equilibrium.

It is convenient and instructive (see [6]) to use a two-dimensional Poincaré section $\Sigma_{u=const}$ to represent these invariant manifolds. The Poincaré section with u constant has the property that trajectories cross it transversally, unless $v = 0$. In particular, the invariant manifolds intersect Σ_u in points or curves, depending on whether the manifold is one- or two-dimensional. In the Poincaré section, we shall easily visualize when a two-dimensional invariant manifold for one equilibrium is bounded by a one-dimensional invariant manifold for a different equilibrium.

Transverse intersections of two-dimensional manifolds correspond to structurally stable heteroclinic orbits between equilibria. In the Poincaré section, these appear as transverse intersections of curves.

We are interested in solutions $(u, v, w)(\xi)$ that reach $u = 0$ at a finite value of ξ. Specifically, we will say a trajectory $(u(\xi), v(\xi), w(\xi)), \xi < \xi_0$ *touches down* at $\xi = \xi_0$ if $u(\xi) \longrightarrow 0+$ as $\xi \longrightarrow \xi_0-$ and $u(\xi) > 0$ for $\xi < \xi_0$. Similarly, we will say $(u(\xi), v(\xi), w(\xi))$ is *unbounded* if $u(\xi) \longrightarrow \infty$ as $\xi \longrightarrow \pm\infty$.

The numerical results were obtained for specific choices of parameters: $s = 2/9$, $D = 0$, $n = 1$. (The choice $n = 1$ was suggested in [17].) The choice of s is intended to be representative of the physical solutions of interest. In case I, different choices of β are considered, while in cases II and III, $\beta = 0.01$ is taken to be representative.

4.1. Case I: Gravity dominates. When gravity dominates, (4.1) has the cubic polynomial flux function

$$f(u) = u^3 + \beta u. \tag{4.4}$$

Note that (4.1) has the symmetry property that it is unchanged by changing the sign of u and ξ. (Then w changes sign, but v does not.)

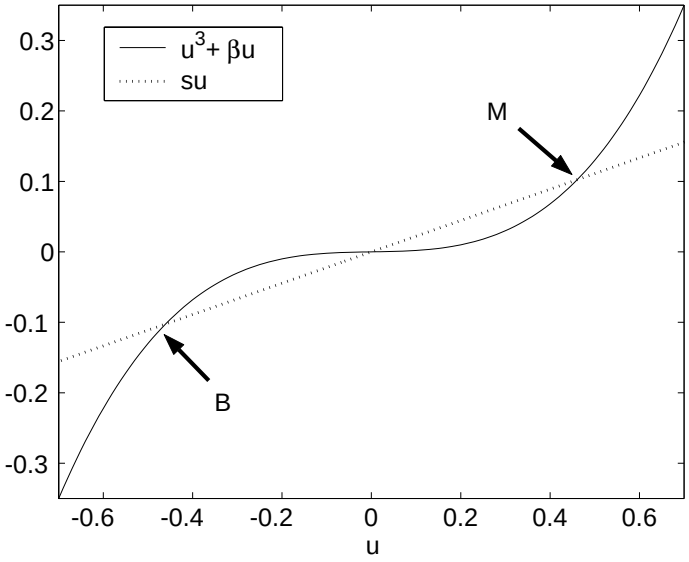

FIG. 4.1. $f(u)$ *and* su.

In Figure 4.1, we show (4.3) for $\beta = 0.01$. The equation has two solutions corresponding to equilibria of (4.1), namely $\overline{u} = \pm\frac{\sqrt{190}}{30}$. (Note that the solution $\overline{u} = 0$ is *not* an equilibrium.) The associated equilibria are

$$B = \left(-\frac{\sqrt{190}}{30}, 0, 0\right), \quad M = \left(\frac{\sqrt{190}}{30}, 0, 0\right).$$

Although B is not physical since it corresponds to negative u, it is nonetheless helpful to consider the associated invariant manifolds.

Linearizing around M, we find the system has two complex conjugate eigenvalues with positive real part (corresponding to a two-dimensional unstable manifold denoted $W^U(M)$), and one real, negative eigenvalue (corresponding to a one-dimensional stable manifold denoted $W^S(M)$). Correspondingly, the equilibrium B

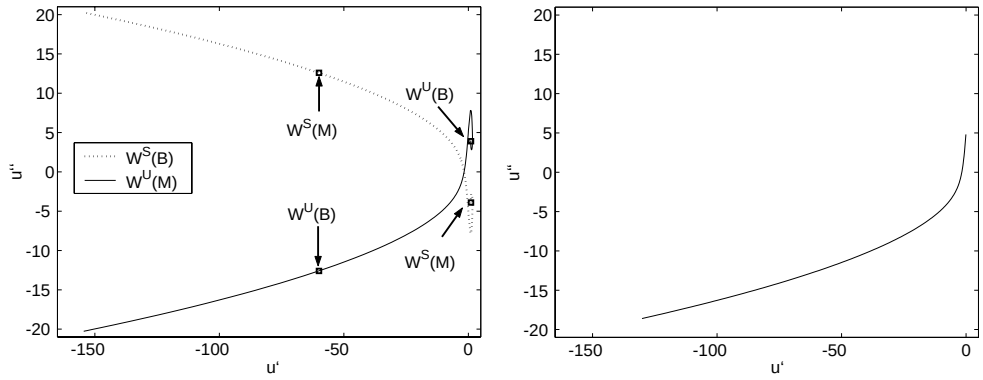

FIG. 4.2. *Case* I *with* $\beta = 0.01$. (a) Σ_0. (b) *Trajectories with a contact line. Shown are only the values at the first intersection with* Σ_0.

has a two-dimensional stable manifold $W^S(B)$ and a one-dimensional unstable manifold $W^U(B)$.

As described in [6, 30], the nature of the two-dimensional manifolds changes from node to focus as the parameter D varies away from zero. In discussing the phase portraits here (with $D = 0$), we consider the focus case only, for which the two associated eigenvalues are complex conjugates. This implies that, near M, solutions along the unstable manifold spiral out. Thus to compute the unstable manifold, we compute trajectories starting from a locus of points along a straight line through M in the tangent plane.

Global picture of phase space. We are interested in how trajectories touch down, so we study the Poincaré section Σ_0 at $u = 0$. By symmetry, the invariant manifolds of B and M are reflections of each other across the plane $u = 0$. The manifolds $W^U(B)$ and $W^S(M)$ are one-dimensional, so they intersect Σ_0 in isolated points, if at all. Each one-dimensional invariant manifold has two connected components, or branches, separated by the equilibrium. Referring to Figure 4.2(a), representing the Poincaré plane $u = 0$, for $\beta = 0.01$, we observe that one branch of $W^U(B)$ intersects Σ_0 twice: first at $(u, u', u'') = (0, 1.06, 3.9)$, then at $(0, -60.0, -12.6)$.[3] The other branch is unbounded at $u = -\infty$ and does not intersect Σ_0. Similarly, one branch of $W^S(M)$ intersects Σ_0 at $(u, u', u'') = (0, 1.06, -3.9)$, while the other branch is unbounded at $u = \infty$ and does not intersect Σ_0.

The two-dimensional manifolds $W^U(M)$ and $W^S(B)$ intersect Σ_0 in curves (see Figure 4.2(a)). $W^U(M)$ is bounded on both ends by the same branch of $W^U(B)$. Near this boundary $W^U(M)$ wraps around $W^U(B)$ an infinite number of times. The spiral of $W^U(M)$ around the first intersection of $W^U(B)$ near $(0, 1.06, 3.9)$ can be seen in Figure 4.2(a). By the time $W^U(B)$ intersects the second time near $(0, -60.0, -12.6)$, the spiral of $W^U(M)$ has become so elongated that it cannot be resolved at this scale.

The points P on Σ_0 of physical interest are those which represent trajectories from M that hit $u = 0$ for the first time at P. These correspond to traveling wave solutions which asymptote to $u = \frac{\sqrt{190}}{30}$ at $\xi = -\infty$ and have a contact line. Although trajectories continue into negative u values, solutions with $u < 0$ are no longer phys-

[3]Here and throughout this section, we give the numerical values of intersection points to one or two decimal places.

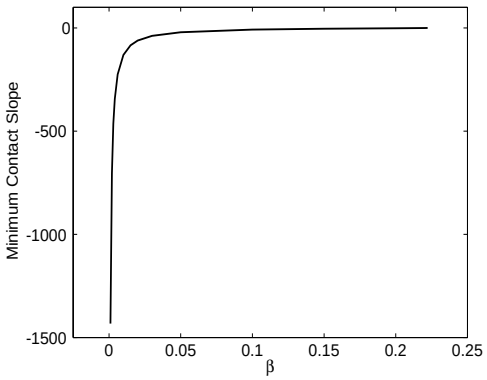

FIG. 4.3. *Minimum slope at $u = 0$ as a function of β, case* I.

ical. All trajectories in $W^U(M)$ hit $u = 0$. The curve of points corresponding to first intersections are shown in Figure 4.2(b). Note that one end of the curve terminates at $u' = 0$. This corresponds to a trajectory that turns around at $u = 0$. This same trajectory eventually winds around to intersect Σ_0 again, this time with a touchdown of slope $u' = -130.1$, corresponding to the other end of the curve shown in Figure 4.2(b). For trajectories inside this orbit, we obtain the finite range of touchdown slopes, spanning $-130.1 \le u' \le 0$. Such large slopes may of course take the model outside its range of validity. However, the slopes here are dimensionless, and may correspond in dimensional variables within the range of the model. This issue is examined in the context of thin film rupture in the paper of Zhang and Lister [42].

Dependence of the range of contact slopes on β. In Figure 4.3, we show how the minimum contact angle varies with the parameter β (from the Navier slip condition (4.2)) in the range $0 < \beta < 2/9$. Keeping $s = 2/9$, $D = 0$, and $n = 1$ fixed, the phase space of solutions is topologically equivalent for $0 < \beta < \frac{2}{9}$. As $\beta \to 0$, M and B approach $(\pm\frac{\sqrt{2}}{3}, 0, 0)$. As β increases from 0, M and B move closer together until all solutions of (4.3) vanish at $\beta = \frac{2}{9}$, where $f'(0) = s$. For all β in this range, the maximum contact slope is zero. The minimum contact slope decreases with decreasing β, as seen above. The plot shows computed values for the minimum value of u' at $u = 0$ for β ranging from 0.001 to 0.22.

4.2. Case II: Marangoni convection dominates. Now consider (4.1) when the Marangoni convection term dominates. In this subsection we consider only $\beta = 0.01$; in this case and in case III we compute solutions only in the physical range $u \ge 0$. The new flux function is quadratic:

$$f(u) = u^2 + \beta. \tag{4.5}$$

For different values of s, the ODE will have zero, one, or two equilibria. The case with $s = 2/9$ is shown in Figure 4.4. The two equilibria are

$$B = \left(\frac{10 - \sqrt{19}}{90}, 0, 0\right), \quad M = \left(\frac{10 + \sqrt{19}}{90}, 0, 0\right).$$

M has a two-dimensional unstable manifold $W^U(M)$ and a one-dimensional stable manifold $W^S(M)$. B has a two-dimensional stable manifold $W^S(B)$ and a one-dimensional unstable manifold $W^U(B)$.

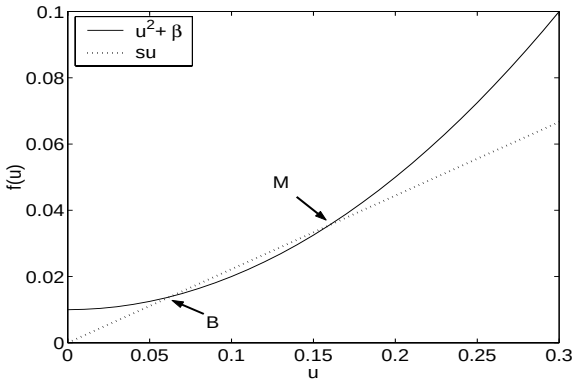

FIG. 4.4. *$f(u)$ and su, case* II*, with $\beta = 0.01$.*

The dynamics at the contact line are now fundamentally different than in the gravity dominated case. The flux function makes the differential equation (4.1) singular at $u = 0$. Note that if (u, v, w) touches down, then $w = u''$ will become unbounded in finite time, so an adaptive time step procedure such as the one we use is essential to capture detailed behavior near $u = 0$. The most important difference from the gravity dominated case is that now trajectories cannot be computed beyond $u = 0$. Thus, trajectories generically fall into two cases: those which touch down in finite time and those which escape to $u = \infty$. Between these two cases are heteroclinic orbits that approach equilibria as $\xi \longrightarrow \pm\infty$.

Global picture of phase space. Since u'' is unbounded at $u = 0$, it is not possible to study Σ_0. Instead, we choose the section $\Sigma_{0.1}$ between B and M. The information about boundaries and dimensions can be read off as before. It is necessary, however, to do further computations to find the range of contact slopes. Intersections of the two-dimensional manifolds again correspond to heteroclinic orbits between equilibria, representing traveling wave solutions with a precursor layer, as in [6].

Both branches of $W^S(M)$ are unbounded. One does not pass $\Sigma_{0.1}$. The other branch intersects $\Sigma_{0.1}$ at $(u, u', u'') = (0.1, 0.16, -0.43)$, narrowly avoids $u = 0$, and intersects again at $(u, u', u'') = (0.1, -2.00, 20.71)$ before heading to $u = \infty$. In contrast, both branches of $W^U(B)$ touch down. One branch does not intersect $\Sigma_{0.1}$. The other intersects first at $(0.1, 0.15, 0.52)$, then at $(0.1, -1.72, -2.02)$ before touching down. These intersection points are labeled in Figure 4.5.

The two-dimensional manifolds $W^U(M)$ and $W^S(B)$ intersect transversally in a single heteroclinic orbit from M to B. Hence the two branches of $W^U(B)$ are boundaries of $W^U(M)$. The curve $W^U(M)$ shown in the Poincaré section of Figure 4.5 represents trajectories that can intersect $\Sigma_0.1$ several times. All trajectories in $W^U(M)$ touch down, with a finite range of contact angles. For the specific parameters $\beta = 0.01$, $s = 2/9$, we find this range to be $-2.436 < u' < -0.464$. Note that, unlike in the gravity driven case, there are no trajectories with contact slope arbitrarily close to 0.

4.3. Case III: The full equation. We now consider the full equation with $\beta = 0.01$ and

$$f(u) = u^2 - u^3 + \beta\left(\frac{2}{3} - u\right). \tag{4.6}$$

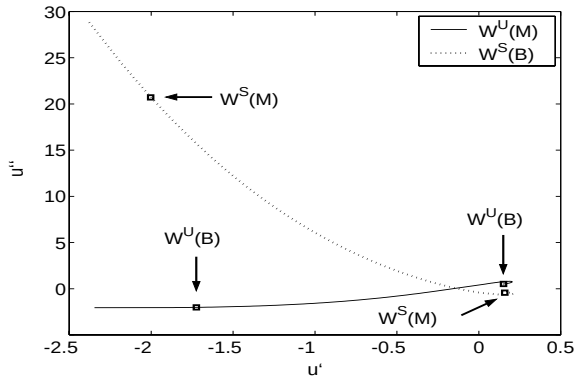

FIG. 4.5. $\Sigma_{0.1}$, *case* II.

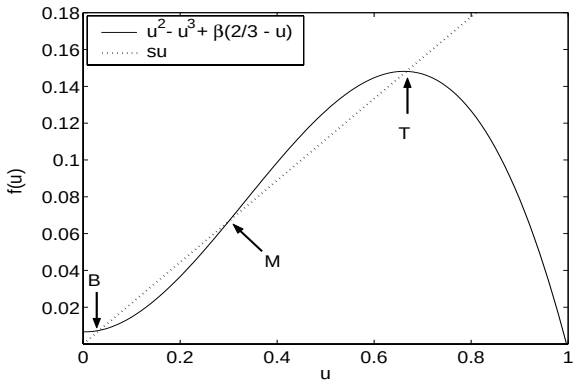

FIG. 4.6. $f(u)$ *and* su, *case* III, $\beta = 0.01$.

See [6] for a parallel discussion of the precursor model case without Navier slip. The flux is now nonconvex, which means the ODE may have one, two, or three equilibria, depending on the value of s. For $s = 2/9$, (4.3) has three solutions. We will find that phase space becomes correspondingly more complicated. The three equilibria (see Figure 4.6) are labeled

$$B = (1/30, 0, 0), \quad M = (3/10, 0, 0), \quad T = (2/3, 0, 0),$$

for bottom, middle, and top. M has a two-dimensional unstable manifold $W^U(M)$ and a one-dimensional stable manifold $W^S(M)$. The other equilibria B and T have two-dimensional stable manifolds $W^S(B), W^S(T)$ and one-dimensional unstable manifolds $W^U(B), W^U(T)$.

As in the case where Marangoni convection dominates gravity, trajectories in the invariant manifolds either will be heteroclinic orbits, unbounded, or will touch down. There is a Lyapunov function that prevents periodic or homoclinic orbits (cf. [6]). Solutions cannot be computed past $u = 0$ since the ODE becomes singular. In what follows, we describe results with respect to the Poincaré section $\Sigma_{0.2}$ between B and M at $u = 0.2$.

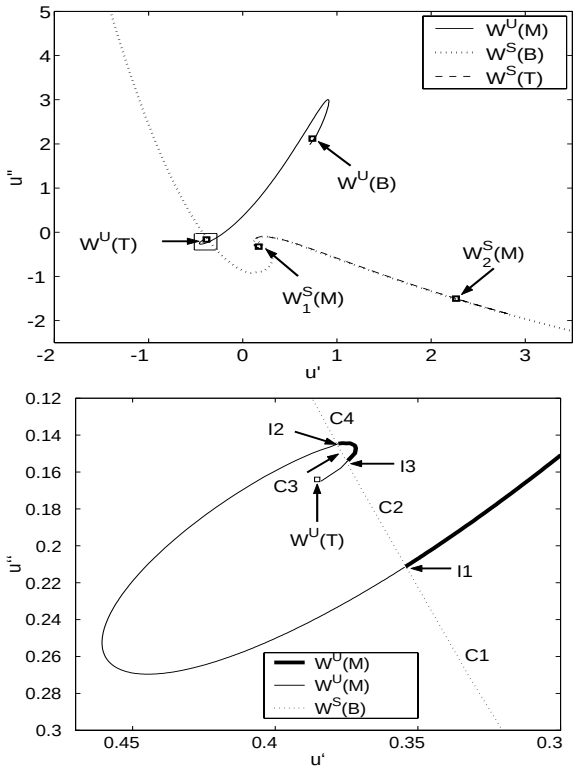

FIG. 4.7. *Case* III. (a) $\Sigma_{0.2}$. (b) *Blow-up of small box in* (a).

The one-dimensional manifolds. $W^U(B)$, $W^U(T)$, and $W^S(M)$ are the one-dimensional invariant manifolds. One branch of $W^U(B)$ touches down and does not pass through $u = 0.2$. The other branch becomes unbounded in u and passes $\Sigma_{0.2}$ at $(0.2, 0.739, 2.120)$. $W^U(T)$ exhibits similar behavior, with an unbounded branch that does not pass through $\Sigma_{0.2}$ and a branch that touches down and hits $\Sigma_{0.2}$ at $(0.2, -0.385, -0.164)$. Both branches of $W^S(M)$ touch down. One branch, $W_1^S(M)$, passes through $\Sigma_{0.2}$ at $(0.2, 0.169, -0.324)$. The other, $W_2^S(M)$, passes through at $(0.2, 2.264, -1.503)$.

The unstable manifold of M. The manifold $W^U(M)$ crosses $W^S(B)$ in three orbits, shown as intersection points in Figure 4.7(b). Note also that $W^U(M)$ wraps infinitely many times around both $W^U(B)$ and $W^U(T)$. These spirals indicate connections from M to both T and B. Connections to B are already evident. Connections to T would appear as an intersection of $W^U(M)$ and $W^S(T)$ in any Poincaré section placed between M and T.

The structure of the intersection of $W^U(M)$ with $W^S(B)$ is shown in more detail in Figure 4.7(b). $W^U(M)$ intersects $W^S(B)$ three times. Each of these intersections I1, I2, and I3 corresponds to a heteroclinic orbit from M to B. Furthermore, $W^S(B)$ divides the qualitative behavior of trajectories on $W^U(M)$. All trajectories on the same side as $W^U(T)$, i.e., between I1 and I2 and between I3 and $W^U(T)$, touch down. All trajectories on the other side, i.e., between $W^U(B)$ and I1 and between I2 and I3, are unbounded.

The stable manifold of T. $W^S(T)$ also has two boundaries, which are the two branches of $W^S(M)$. The spiral at $W_1^S(M)$ can be seen clearly, while the spiral at $W_2^S(M)$ is four orders of magnitude longer than it is wide, and requires corresponding resolution to be seen.

The stable manifold of B. Each trajectory on the stable manifold of B (which hits $\Sigma_{0.2}$) comes out from $B = (1/30, 0, 0)$, passes through $u = 0.2$, turns around, and hits $u = 0.2$ again before touching down. Thus each trajectory appears as two points on $\Sigma_{0.2}$. $W^S(B)$ is split by $W^U(M)$ into four distinctly behaving sheets which we label C1, C2, C3, and C4.

The sheet C1 approaches the heteroclinic orbit I1 at one end and wraps around $W_1^S(M)$ at the other. The sheet wraps back on itself around $(0.2, 0, -1)$. Each trajectory has one point between I1 and $(0.2, 0, -1)$ (where u is increasing) and one point between $(0.2, 0, -1)$ and $W_1^S(M)$ (where u is decreasing). Trajectories which pass very close to I1 going out also pass very close to $W^S(M)$ coming back. In fact, C1 spirals around $W_1^S(M)$ infinitely many times.

Outgoing trajectories in C2 are bounded by I1 and I3. The trajectories which pass very close to I1 spiral around $W_2^S(M)$ on their second pass, and the trajectories which pass very close to I3 spiral around $W_1^S(M)$ when they return. Trajectories between these two boundaries are very close to $W^S(T)$ on their return.

Outgoing trajectories on C3 are bounded by I3 and I2. Trajectories that pass near both of these orbits on the way out spiral tightly around $W_2^S(M)$ on their way back. Trajectories between the two boundaries form a thin loop that follows $W^S(T)$ very closely, and stretches down to $(0.2, 2.84, -1.86)$.

Finally, outgoing trajectories on C4 are bounded on one side by I2. The trajectories which pass near to I2 spiral tightly around $W_1^S(M)$ on their return journey. Trajectories which pass further away from C1 return in a line that follows $W^S(T)$ and eventually stretches beyond it.

Note that both $W_1^S(M)$ and $W_2^S(M)$ have quadruple spirals, that is, four sheets wrapping around them infinitely many times. $W_1^S(M)$ has one boundary each of $W^S(T)$, C1, C2, and C4, whereas $W_2^S(M)$ has one boundary each from $W^S(T)$ and C2, and two from C3.

4.4. Connection to the asymptotics. In the computations for case III, for a given wave speed s, we find a one-parameter family of trajectories that touch down. Here we relate this one-parameter family to the two-parameter family of local touch down solutions given by the asymptotics of section 2. Specifically for $s = 2/9$, we find a finite range of values for the parameter a in the asymptotic solution.

With the scaling $\xi - \xi_0 = -(\frac{2}{3})^{1/3}x$ of section 2, the asymptotic expansion about a point $\xi = \xi_0$ of touchdown becomes

$$h(\xi) = -a\left(\frac{2}{3}\right)^{\frac{1}{3}}\eta + \frac{1}{2a}\left(\frac{2}{3}\right)^{\frac{2}{3}}\eta^2 \log\left(-\left(\frac{2}{3}\right)^{\frac{1}{3}}\eta\right) + b\left(\frac{2}{3}\right)^{\frac{2}{3}}\eta^2 + \text{h.o.t.}, \tag{4.7}$$

in which $\eta = \xi - \xi_0 < 0$. In particular, the contact slope is given by $v(\xi_0) = -a\left(\frac{2}{3}\right)^{1/3}$. We can read off the limiting value of $v(\xi)$ as u approaches zero and thus obtain the value of a. Corresponding values for b also come from the form (1.2). Specifically, we find

$$w = u'' = \frac{1}{a}\left(\frac{2}{3}\right)^{\frac{2}{3}} \log\left(-\left(\frac{2}{3}\right)^{\frac{1}{3}}\eta\right) + \frac{3}{2a}\left(\frac{2}{3}\right)^{\frac{2}{3}} + 2\left(\frac{2}{3}\right)^{\frac{2}{3}} b + \text{h.o.t.} \tag{4.8}$$

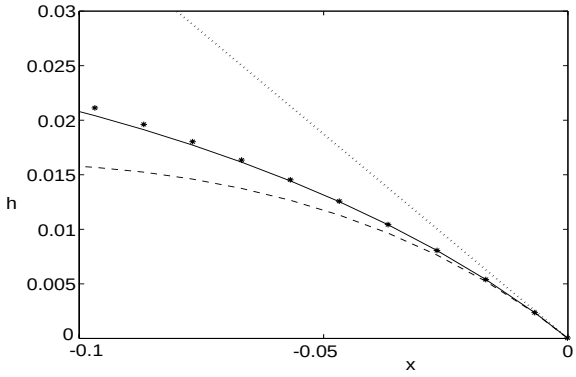

FIG. 4.8. *.....first order, - - -second order, *****third order, a=0.429, b=0.762.*

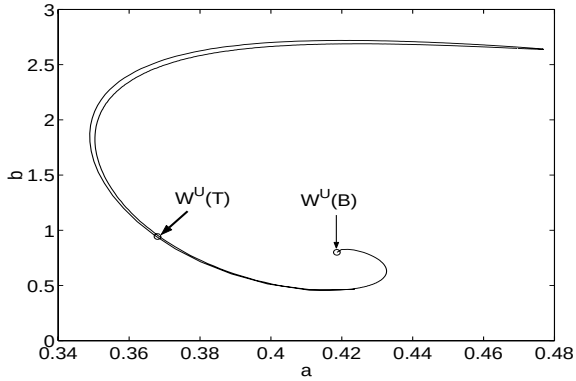

FIG. 4.9. *Asymptotic parameters a and b.*

Thus,

$$e^{\left(a\left(\frac{3}{2}\right)^{2/3}w(\xi)\right)} \approx -\left(\frac{2}{3}\right)^{1/3} e^{\left(\frac{3}{2}+2ab\right)}(\xi-\xi_0). \tag{4.9}$$

Consequently, $e^{\left(a\left(\frac{3}{2}\right)^{2/3}w(\xi)\right)}$ approaches a constant slope m as u approaches zero. Computing this value of m from the calculated trajectory, and the parameter a as above, the expression

$$m = -\left(\frac{2}{3}\right)^{1/3} e^{\left(\frac{3}{2}+2ab\right)} \tag{4.10}$$

determines b. In Figure 4.8, we show a sample comparison between the first three terms of the asymptotic expansion with the corresponding numerical solution of the full equation, with parameters a, b calculated as described above.

Range of *a* and *b*. Plotting the two asymptotic parameters a and b against each other, for all trajectories on $W^U(M)$ which touch down, gives a curve in the (a, b) plane. Consider the close up Poincaré section of the intersection between $W^U(M)$ and $W^S(B)$. In Figure 4.9, we show this curve for points on $W^U(M)$ between I1 and

I2 corresponding to trajectories that touch down in finite time. Points adjacent to I_1 and I_2 correspond to identical values of a and b, in fact, the same values as for the branch of $W^U(B)$ that touches down. The curve in Figure 4.9 varies smoothly but very nearly doubles back on itself. Trajectories near the heteroclinic orbits approach B and then shoot off along $W^U(B)$.

The points along $W^U(M)$ from I3 to $W^U(T)$ give another one-parameter family of solutions. Their a, b values range continuously from the a, b value of the branch of $W^U(B)$ that touches down (since I2 is another heteroclinic orbit) to the a, b value of the branch of $W^U(T)$. This second curve closely follows the first one.

5. Discussion. In this section, we discuss the significance of the results for the traveling wave problem and the moving contact line. The most striking conclusion from our numerical results is that for each of the three problems considered, there is a limited range of contact angles. This particular observation has not been noted in previous studies of the traveling wave problem with slip [31, 38] for the case of gravity driven films. For the Marangoni cases II and III the effect is even more pronounced; the range does not include a zero contact angle, in contrast to well-known results for (2.12) without convection (i.e., $f = 0$) for both traveling waves [9] and weak solutions of the full PDE [8, 3]. For example, in case I, Figure 4.2(b), for each contact slope u' in the range $(-130.1, 0]$, there is a unique traveling wave solution that touches down with that slope. In contrast, in case III, not only are there no traveling waves that touch down with zero slope, but for each slope in the range there can be more than one traveling wave with that touchdown slope, as demonstrated in Figure 4.9.

In experiments, the contact line speed is often observed to be related to the dynamic contact angle or the slope of the film as the thickness approaches zero. For the model, this would result in a boundary condition relating the contact angle to the speed of the wave. Since the upstream thickness is related to the speed s via (2.17), for traveling waves, such a boundary condition becomes a relationship between upstream thickness and contact angle. In case I, the boundary condition would select a unique traveling wave, provided the contact slope is in the admissible range. However, in case III, such a law does not in general select a unique traveling wave. A similar nonuniqueness was found for the precursor model [6] in the case of gravity and opposing Marangoni stress.

There is also the issue of whether the contact angle should be related to the slope of the free surface at zero height, or to an observed slope, that might be taken to be the maximum slope, generally slightly away from the contact line itself. There is much discussion of this issue in the literature (see [25, 26] and the references therein). The Navier slip condition is an attempt to incorporate in a continuum model the physical effects at the molecular scale. For this reason, the asymptotic results apply strictly at the contact line. As in [25], it would be possible to carry out matched asymptotics to relate the asymptotic solution at zero height to solutions of the full problem away from a small neighborhood of the contact line. In this paper, we have instead compared numerical solutions with the asymptotic solution; the discussion above is based on this comparison.

Case III is particularly interesting because of the nonconvex flux and the connection to compressive and undercompressive waves discussed in [6]. The notion of compressive and undercompressive carries over to this paper in the following way: we call trajectories from M that touch down compressive traveling waves. If the trajectory from T touches down, we refer to it as an undercompressive wave. Unlike the precursor model in [6], we do not have characteristics ahead of the wave, hence these

names are used to distinguish between cases where characteristics from the bulk film go into the contact line (compressive) or come out of the contact line (undercompressive). In the former case, information from the bulk can influence the contact line. In the latter case, information from the contact line is carried into the bulk.

Note that there is a range of speeds for which we have three equilibria B, M, and T. We conjecture that for speeds in an interval within this range, one branch of the unstable manifold from T touches down to $u = 0$. Each such trajectory will have a touchdown angle. It would be interesting to know if a given boundary condition at the contact line selects a unique undercompressive wave.

It would be interesting to consider the traveling waves that touch down in the context of the dynamic free boundary problem for the PDE (2.12). We expect that the structure of case III is as rich as that for the precursor model [6, 4]. The contact line raises a new issue: that of how to treat the free boundary for the full PDE. The full nonlinear dynamics have not been explored, with the exception of [35], in which a special case of the PDE without convection was studied.

Acknowledgment. We gratefully acknowledge helpful discussions with David Schaeffer.

REFERENCES

[1] W. D. Bascom, R. L. Cottington, and C. R. Singleterry, *Dynamic surface phenomena in the spontaneous spreading of oils on solids*, in Contact Angle, Wettability and Adhesion, F. M. Fowkes, ed., American Chemical Society, Washington, DC, 1964, pp. 355–379.

[2] E. Beretta, J. Hulshof, and L. A. Peletier, *On an ODE from forced coating flow*, J. Differential Equations, 130 (1996), pp. 247–265.

[3] E. Beretta, M. Berstch, and R. Dal Passo, *Nonnegative solutions of a fourth order nonlinear degenerate parabolic equation*, Arch. Ration. Mech. Anal., 129 (1995), pp. 175–200.

[4] A. Bertozzi, A. Münch, M. Shearer, and K. Zumbrun, *Stability of compressive and undercompressive thin film travelling waves*, European J. Appl. Math., 12 (2001), pp. 253–291.

[5] A. L. Bertozzi, A. Münch, X. Fanton, and A. M. Cazabat, *Contact line stability and 'undercompressive shocks' in driven thin film flow*, Phys. Rev. Lett., 81 (1998), pp. 5169–5172.

[6] A. L. Bertozzi, A. Münch, and M. Shearer, *Undercompressive shocks in thin film flows*, Phys. D, 134 (1999), pp. 431–464.

[7] A. L. Bertozzi and M. Shearer, *Existence of undercompressive traveling waves in thin film equations*, SIAM J. Math. Anal., 32 (2000), pp. 194–213.

[8] A.L. Bertozzi and M. Pugh, *The lubrication approximation for thin viscous films: Regularity and long time behavior of weak solutions*, Comm. Pure Appl. Math., 49 (1996), pp. 85–123.

[9] S. Boatto, L. Kadanoff, and P. Olla, *Travelling wave solutions to thin film equations*, Phys. Rev. E, 48 (1993), p. 4423.

[10] J. B. Brzoska, F. Brochard-Wyart, and F. Rondelez, *Exponential growth of fingering instabilities of spreading films under horizontal thermal gradients*, Europhys. Lett., 19 (1992), pp. 98–102.

[11] A. M. Cazabat, F. Heslot, S. M. Troian, and P. Carles, *Finger instability of this spreading films driven by temperature gradients*, Nature, 346 (1990), pp. 824–826.

[12] P. G. de Gennes, *Wetting: Statics and dynamics*, Rev. Mod. Phys., 57 (1985), p. 827.

[13] E. B. Dussan V and S. Davis, *On the motion of a fluid–fluid interface along a solid surface*, J. Fluid Mech., 65 (1974), pp. 71–95.

[14] P. Ehrhard and S. H. Davis, *Non-isothermal spreading of liquid drops on horizontal plates*, J. Fluid. Mech., 229 (1991), pp. 365–388.

[15] S. Goldstein, ed., *Modern Developments in Fluid Dynamics*, Vol. 2, Dover, New York, 1965.

[16] A. A. Golovin, B. Y. Rubinstein, and L. M. Pismen, *Effect of van der waals interaction on the fingering instability of thermally driven thin wetting films*, Langmuir, 17 (2001), pp. 3930–3936.

[17] H. P. Greenspan, *On the motion of a small viscous droplet that wets a surface*, J. Fluid Mech., 84 (1978), pp. 125–143.

[18] P. J. Haley and M. J. Miksis, *The effect of the contact line on droplet spreading*, J. Fluid Mech., 223 (1991), pp. 57–81.
[19] L. Hocking, *Spreading and instability of a viscous fluid sheet*, J. Fluid Mech., 221 (1990), pp. 373–392.
[20] L. M. Hocking, *A moving fluid interface on a rough surface*, J. Fluid Mech., 76 (1976), pp. 801–817.
[21] L. M. Hocking, *A moving fluid interface. Part* 2. *The removal of the force singularity by a slip flow*, J. Fluid Mech., 79 (1977), pp. 209–229.
[22] L. M. Hocking, *The spreading of a thin drop by gravity and capillarity*, Quant. J. Mech. Appl. Math., 36 (1983), pp. 55-69.
[23] L. M. Hocking, *Rival contact-angle models and the spreading of drops*, J. Fluid. Mech., 239 (1992), pp. 671–681.
[24] H. Huppert, *Flow and instability of a viscous current down a slope*, Nature, 300 (1982), pp. 427–429.
[25] S. Kalliadasis and H.-C. Chang, *Apparent dynamic contact angle of an advancing gas-liquid meniscus*, Phys. Fluids, 6 (1994), pp. 12–23.
[26] S. Kalliadasis and H.-C. Chang, *Dynamics of liquid spreading on solid surfaces*, Ind. Eng. Chem. Res., 35 (1996), pp. 2860–2874.
[27] D. E. Kataoka and S. M. Troian, *A theoretical study of instabilities at the advancing front of thermally driven coating films*, J. Coll. Int. Sci., 192 (1997), pp. 350–362.
[28] D. E. Kataoka and S. M. Troian, *Stabilizing the advancing front of thermally driven climbing films*, J. Coll. Int. Sci., 203 (1998), pp. 335–344.
[29] V. Ludviksson and E. N. Lightfoot, *The dynamics of thin liquid films in the presence of surface-tension gradients*, Am. Inst. Chem. Engrs. J., 17 (1971), pp. 1166–1173.
[30] A. Münch, *Shock transitions in Marangoni-gravity driven thin film flow*, Nonlinearity, 13 (2000), pp. 731–746.
[31] A. Münch and B. Wagner, *Numerical and asymptotic results on the linear stability of a thin film spreading down a slope of small inclination*, European J. Appl. Math., 10 (1999), pp. 297–318.
[32] C. Navier, *Memoire sur les lois du mouvement des fluids*, Memoires de l'Academie Royale des Sciences de l'Institut de France, 6 (1823), pp. 389–440.
[33] P. Neogi and C. A. Miller, *Spreading kinetics of a drop on a rough solid surface*, J. Coll. Int. Sci., 92 (1983), pp. 338–349.
[34] A. Oron, S. H. Davis, and S. G. Bankoff, *Long-scale evolution of thin liquid films*, Rev. Mod. Phys., 69 (1997), pp. 931–980.
[35] F. Otto, *Lubrication approximation with prescribed nonzero contact angle*, Comm. Partial Differential Equations, 23 (1998), pp. 2077–2164.
[36] M. Schneemilch and A. M. Cazabat, *Shock separation in wetting films driven by thermal gradients*, Langmuir, 16 (2000), pp. 9850–9856.
[37] M. Schneemilch and A. M. Cazabat, *Wetting films in thermal gradients*, Langmuir, 16 (2000), pp. 8796–8801.
[38] M. A. Spaid and G. M. Homsy, *Stability of Newtonian and viscoelastic dynamic contact angles*, Phys. Fluids, 8 (1996), pp. 460–478.
[39] E. O. Tuck and L. W. Schwartz, *A numerical and asymptotic study of some third-order ordinary differential equations relevant to draining and coating flows*, SIAM Rev., 32 (1990), pp. 453–469.
[40] O. V. Voinov, *Inclination angles of the boundary in moving liquid layers*, Zh. Prikl. Mekh. Tekh. Fiz., 2 (1977), pp. 92–99.
[41] M. B. Williams and S. H. Davis, *Nonlinear theory of film rupture*, J. Coll. Int. Sci., 90 (1982), pp. 220–228.
[42] W. W. Zhang and J. R. Lister, *Similarity solutions for van der Waals rupture of a thin film on a solid substrate*, Phys. Fluids, 11 (1999), pp. 2454–2462.